Journal of Materials Processing Technology xxx (2011) xxx–xxx

Contents lists available at ScienceDirect

Journal of Materials Processing Technology

journal homepage: www.elsevier.com/locate/jmatprotec

Role of friction on the thermal development in ultrasonically consolidated aluminum foils and composites

Steve Koellhoffer[a], John W. Gillespie Jr.[a,1], Suresh G. Advani[a,*], Travis A. Bogetti[b]

[a] Center for Composite Materials, University of Delaware, Newark, DE 19716, United States
[b] Army Research Laboratory, Aberdeen Proving Grounds, Maryland, 21005, United States

ARTICLE INFO

Article history:
Received 17 January 2011
Received in revised form 9 June 2011
Accepted 11 June 2011
Available online xxx

Keywords:
Ultrasonic consolidation
Aluminum
Friction coefficient
Metal matrix composite

ABSTRACT

Ultrasonic consolidation is a solid-state bonding process capable of producing metal and metal matrix composite parts. In this work a friction-based heat generation model is proposed to characterize the thermal development of ultrasonically consolidated aluminum foils and continuous fiber alumina reinforced aluminum metal matrix composite tape as a function of process control parameters. The friction coefficient between mating surfaces is determined experimentally, and the credibility of using both a constant friction coefficient and a process dependent friction coefficient is assessed. In most cases a constant friction coefficient is capable of producing results that are within 15% error; while a process dependent friction coefficient achieves an average error of 7%.

© 2011 Elsevier B.V. All rights reserved.

1. Introduction

Ultrasonic consolidation (UC) is a low temperature bonding process that can be used in the fabrication of metal and metal matrix composite (MMC) parts. Layers of metallic films (foils or prepreg MMC tape) are built up on top of each other forming the desired shape; this is synonymous to the methodology used in automated tape placement (ATP) currently employed in the thermoplastic tape lamination industry in use by aerospace companies. Tierney and Gillespie (2006) investigated and modeled the in situ strength development of the thermoplastic ATP process. By building up thin successive layers and avoiding bulk heating, residual stresses from fabrication are reduced. UC provides many advantages over traditional liquid processing methods typically employed in the manufacture of composites as discussed by Doumanidis and Gao (2004). Weld temperatures are typically below 50% of the melt temperature and the time at this temperature is very short (0.02–0.72 s), thus allowing materials to retain much of their preprocessed crystallography. Upon inspection of the post weld interface there is often no indication of melting or recrystallization for low temperature welds; this has been observed by both Yang et al. (2009) and Clews (2009). However, Clews does state that microstructural changes could readily occur given the right combination of temperature and time. Such is likely the case for welds made by Mariani and Ghassemieh (2010). Mariani and Ghassemieh welded at speeds of 34.5 mm/s and predicted high temperatures to be 50–80% of the melt temperature (330–528 °C). For these hotter foil–foil welds some microstructural changes were visible as Mariani and Ghassemieh observed recrystallization in a thin layer (5 μm band) at the weld interface, between 100 μm foils, using electron backscatter diffraction. Largely retained crystallography and minimal residual stress buildups introduced by tape lamination may reduce or eliminate the need for costly post-processing heat treatments. Localized heating, versus bulk heating, also helps reduce processing costs by decreasing the amount of energy required during fabrication. Additionally, low temperature layered processing facilitates the use and placement of thermally sensitive materials (e.g. embedded sensors and fibers) that could be otherwise damaged or imprecisely placed using liquid processing. This has been demonstrated by various researchers. Cheng et al. (2007) successfully embedded nickel based thin film thermocouples into copper work pieces via UC. Siggard et al. (2006) consolidated USB-based sensors into aluminum. Kong et al. (2004b) embedded shape memory alloy (SMA) fibers into aluminum to create adaptive structures for aerospace applications. After embedding SMA fibers, Kong and Soar built upon their previous work by using SiC (2005a) for structural applications and optical fibers (2005b) for data transport. With UC it is also possible to weld a variety of dissimilar materials including: aluminum, brass, stainless steel, super alloys, SiC fiber, and MMC tape. Janaki Ram et al. (2007) consolidated many of

* Corresponding author at: George W. Laird Professor of Mechanical Engineering, United States.
E-mail address: advani@udel.edu (S.G. Advani).
[1] Address: Donald C. Phillips Professor of Civil and Environmental Engineering, Department of Materials Science and Engineering/Department of Civil and Environmental Engineering, United States.

0924-0136/$ – see front matter © 2011 Elsevier B.V. All rights reserved.
doi:10.1016/j.jmatprotec.2011.06.011

Please cite this article in press as: Koellhoffer, S., et al., Role of friction on the thermal development in ultrasonically consolidated aluminum foils and composites. J. Mater. Process. Tech. (2011), doi:10.1016/j.jmatprotec.2011.06.011

Report Documentation Page

Form Approved
OMB No. 0704-0188

Public reporting burden for the collection of information is estimated to average 1 hour per response, including the time for reviewing instructions, searching existing data sources, gathering and maintaining the data needed, and completing and reviewing the collection of information. Send comments regarding this burden estimate or any other aspect of this collection of information, including suggestions for reducing this burden, to Washington Headquarters Services, Directorate for Information Operations and Reports, 1215 Jefferson Davis Highway, Suite 1204, Arlington VA 22202-4302. Respondents should be aware that notwithstanding any other provision of law, no person shall be subject to a penalty for failing to comply with a collection of information if it does not display a currently valid OMB control number.

1. REPORT DATE	2. REPORT TYPE	3. DATES COVERED
2011		**00-00-2011 to 00-00-2011**

4. TITLE AND SUBTITLE	5a. CONTRACT NUMBER
Role Of Friction On The Thermal Development In Ultrasonically Consolidated Aluminum Foils And Composites	5b. GRANT NUMBER
	5c. PROGRAM ELEMENT NUMBER
6. AUTHOR(S)	5d. PROJECT NUMBER
	5e. TASK NUMBER
	5f. WORK UNIT NUMBER
7. PERFORMING ORGANIZATION NAME(S) AND ADDRESS(ES) **Army Research Laboratory,Aberdeen Proving Grounds,MD,21005**	8. PERFORMING ORGANIZATION REPORT NUMBER
9. SPONSORING/MONITORING AGENCY NAME(S) AND ADDRESS(ES)	10. SPONSOR/MONITOR'S ACRONYM(S)
	11. SPONSOR/MONITOR'S REPORT NUMBER(S)

12. DISTRIBUTION/AVAILABILITY STATEMENT
Approved for public release; distribution unlimited

13. SUPPLEMENTARY NOTES
Journal of Materials Processing Technology, Preprint, 14 pages

14. ABSTRACT
Ultrasonic consolidation is a solid-state bonding process capable of producing metal and metal matrix composite parts. In this work a friction-based heat generation model is proposed to characterize the thermal development of ultrasonically consolidated aluminum foils and continuous fiber alumina reinforced aluminum metal matrix composite tape as a function of process control parameters. The friction coefficient between mating surfaces is determined experimentally, and the credibility of using both a constant friction coefficient and a process dependent friction coefficient is assessed. In most cases a constant friction coefficient is capable of producing results that are within 15% error; while a process dependent friction coefficient achieves an average error of 7%.

15. SUBJECT TERMS

16. SECURITY CLASSIFICATION OF:			17. LIMITATION OF ABSTRACT	18. NUMBER OF PAGES	19a. NAME OF RESPONSIBLE PERSON
a. REPORT	b. ABSTRACT	c. THIS PAGE			
unclassified	**unclassified**	**unclassified**	**Same as Report (SAR)**	**15**	

these material combinations and investigated the bonding through microscopy.

Fig. 1 is a schematic of the key elements involved in UC.

The cylindrical horn (also referred to as the *sonotrode*) applies a normal force, F, which brings the top tape in contact with the material to which it will be bonded. Sufficient force is required to ensure intimate contact at the interface. Processing time, t, is controlled by the contact length (the longitudinal distance over which force is applied), l_c, and linear weld speed (tangential speed at the horn's surface, determined via the horn's RPM and diameter), s. s and t are defined by Eqs. (1) and (2).

$$s = \pi D \frac{RPM}{60} \tag{1}$$

$$t = \frac{l_c}{s} \tag{2}$$

The horn oscillates at a fixed frequency of 20 kHz, f, and peak-to-peak amplitude, λ. The number of oscillation cycles, N, a sample is subjected to for any given weld is determined by:

$$N = tf = \frac{fl_c}{s} \tag{3}$$

The surface of the horn is knurled. This provides a firm grip between the horn and the upper tape thus preventing slip, and consequently welding, at the tool–tape interface. Thereby relative motion occurs between the upper tape and the substrate resulting in frictional work. Friction causes abrasion of the contacting surfaces smoothing out irregularities, breakup and dispersion of surface oxides and asperities, and heat generation from dissipated frictional work which all promote bonding and welding. Additional details regarding the specifications of the welder used in this study as well as the materials processed will be given in the equipment and materials section.

The exact bonding mechanisms involved in UC are not well defined. It has been suggested that diffusion and plastic deformation aid in the bonding process as theorized by Neppiras (1965) and discussed by Hazlett and Ambekar (1970). Janaki Ram et al. (2007) attributed flow lines to plastic deformation which permitted the embedment of fibers during UC. Yang et al. (2009) has utilized various optical techniques (orientation imaging microscopy, OIM, and X-ray energy dispersive spectroscopy, EDS) that quantified the presence of plastic deformation and diffusion during UC. It is also known that the bonding mechanisms of ultrasonic welding are heat-assisted. Though not required, the application of additional heat (pre-heating) facilitates the welding process as reported by Neppiras (1965). Plastic deformation occurs from friction, the applied load, and thermal and acoustic softening. Acoustic softening can result when a material is subjected to high frequency loads. Langenecker (1966) showed that the effects of ultrasonic exposure has much the same effect as elevated temperatures do on the yield strength through the comparison of stress vs. elongation plots at varying temperature and ultrasonic energy levels. In turn, this makes localized plastic deformation occur more readily which is required to bring mating surfaces together and fill the gaps. Gaps can be naturally occurring due to material variation or induced by embedding materials (e.g. fibers, sensors, etc.). While some material mixing may occur providing a mechanical bond from plastic flow, the experimentally measured concentration gradients obtained through EDS by Gunduz et al. (2005) and Mariani and Ghassemieh (2010) suggest diffusion occurs along the boundaries between materials producing superior atomic bonds. However, since surfaces must be in close contact, the applied pressure and plastic deformation aid diffusion. Diffusion is a temperature dependent process, as is yield strength, thus the processing temperature and weld time are important factors in the bonding process.

Temperature increases are attributed to two sources: bulk plastic deformation, and interfacial friction. The latter being the focus of this paper. It is assumed that slip occurs at the interface between materials being consolidated for the entire duration of the welding process, which promotes friction and deformation of material at the weld's interface. For this study thermal contributions from deformation are neglected and only frictional contributions are accounted for.

1.1. Deformational heat

Thermal contributions from deformation are negligible for several reasons; though, this is not immediately obvious. To assess the amount of heat generated by deformation the amount of plastic work needs to be determined. Plastic work per unit volume can be described by the product of the yield stress and the change in plastic strain developed. If the entire sample flowed plastically without slipping, and all plastic work was dissipated as heat, deformational heat generation could produce approximately five times the energy of the frictional contribution presented in this paper (see Section 2.1 for heat generation flux derivation), assuming normal room temperature properties. However, numerous factors limit and diminish the ability for deformation to contribute significantly to the thermal development during UC of foils and tapes. Small temperature gradients through the material's thickness will cause a gradient of the yield stress. The weld's interface temperature will be the highest (either from localized plastic deformation and/or friction). Areas of highest temperature will have the lowest yield strength. By accounting for a small amount of thermal variation it is expected that only material near the interface will yield plastically. This has been confirmed experimentally. The entire bulk material does not flow plastically. In a technical report promoting UC White (2003) stated that Plastic flow is confined to a thin interfacial layer 10–20 μm thick, which is at most 10% of the sample's thickness. This was proven through grain boundary mapping of the cross-section of a consolidated sample by means of electron backscatter diffraction analysis by Mariani and Ghassemieh (2010) in their microstructural investigation of UC Al. For the case of MMC tape in this study only the matrix will accumulate plastic strain as the brittle ceramic fiber reinforcement would break if yielded plastically. Thus the volume of material behaving plastically is further reduced via the fiber volume fraction. Inside the plastic zone, only 33% of the plastic work is expected to be converted into heat for UC aluminum (for non-UC plastic deformation typically 90% conversion is assumed). The remaining energy is stored in the material's microstructure. This assumption is also used in Zhang and Li's (2009) dynamic thermal–mechanical model of the first 0.0025s of an ultrasonic weld and is based upon the work by Hodowany (1997) and Ravichandran et al. (2002). Hodowany (1997) and Ravichandran et al. (2002) carried out experiments measuring the percentage of work dissipated as heat as a function of the plastic strain developed. As a consequence of the aforementioned factors present in UC the potential contribution of deformation is reduced from 458% of the frictional contribution to 6%. Further reduction of the deformational heat contribution results from the decrease in material strength. As stated in Hibbeler's (2002) textbook, using a perfectly plastic material model, the stress level performing work will be limited by the materials yield strength. The experimental results shown in Langenecker's (1966) tensile testing indicated both elevated temperatures and the presence of ultrasonic energy significantly decreases the yield strength of Aluminum. For UC conditions similar to this study the reduction in yield stress from mild heating (100 °C) and typical ultrasonic softening (20,000 W/m^2) is on the order of 80% as indicated by Siddiq and Ghassemieh (2009) in their theoretical analysis investigating the thermal and acoustic softening exhibited during UC. Consequently, deformational

Please cite this article in press as: Koellhoffer, S., et al., Role of friction on the thermal development in ultrasonically consolidated aluminum foils and composites. J. Mater. Process. Tech. (2011), doi:10.1016/j.jmatprotec.2011.06.011

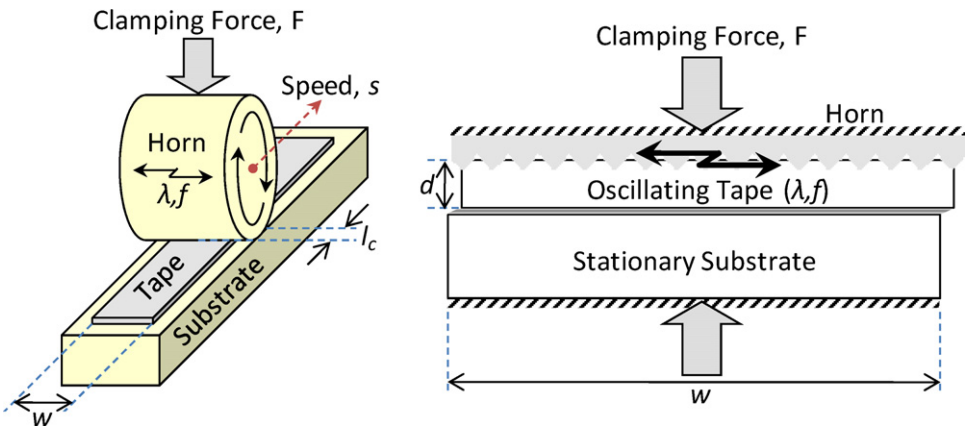

Fig. 1. UC Schematic: left, isometric view of a tape being welded to a substrate; right, through-thickness cross-section of tape and substrate.

contributions are reduced to approximately 1% (for MMC tape) of the frictional contribution using this simplified calculation. For 6061-T6 foils this increases to 7%, and for 3003-H18, 4%. In 2009, Zhang and Li proposed a more detailed theoretical dynamic FEA simulation of the UC process which also supports the conclusion that deformational energy is negligible; after the 20th oscillatory cycle (0.001 s) the plastic heat generation rate saturated and contributed to only 0.3% (for 3003-H18, σ_y = 186 MPa) of any additional heat accumulated at the weld's interface. The back of the envelope calculation performed in this section assumes uniform stress across the width (vs. three dimensional) and does not allow slip; consequently, it is a very conservative, upper limit, approach to approximating the potential contribution of deformational heat relative to frictional heating.

Since deformation is a negligible thermal contributor the objective of this work is to explore the role of friction in increasing the interface temperature and its dependence on the machine variables such as speed, amplitude and applied force. Section 2 will propose a model to relate temperature through energy balance to the friction coefficient. The value of the friction coefficient will be determined by conducting experiments under various speeds, applied forces and amplitudes on an ultrasonic welder and by matching the experimental temperatures measured with an IR camera with model predictions. Some of the challenges in this characterization technique will be outlined.

1.2. Friction

Friction is the resulting force that opposes motion between two contacting surfaces. In Bowden and Tabor's (1950) book, much work, experimentally and theoretically, was done to advance the understanding of the mechanisms involved in the friction and lubrication of solids. They report that the classical expression quantifying friction, Eq. (4), dates back as far as Leonardo da Vinci, but most credit it to the work of Amontons and Coulomb. The law states that the force of sliding friction, F_{fr}, is proportional to its normal force, F_N. The constant of proportionality, μ, is interchangeably referred to as the coefficient of friction or the friction coefficient.

$$F_{fr} = \mu F_N \tag{4}$$

1.2.1. Friction coefficient variability and trends

The friction coefficient is a dimensionless parameter determined experimentally that quantifies the effects of a variety of elements that influence the resistance to slip between materials. Blau (2009) wrote a more modern book referencing much of the more modern studies and standards pertaining to friction. An underlying theme of the book is that beyond material properties and surface characteristics there is a plethora of factors that influence the coefficient of friction, several of which vary during UC. The input parameters involved in welding are clamping force, F, oscillation amplitude, λ, and weld speed, s. All of these, as well as temperature, have been shown to influence the friction coefficient.

Clamping force, F, is proportionally related to the applied pressure through the contact area, $l_c w$, so any influence pressure may have on the friction coefficient will be evinced by variations in F. In cyclic fretting fatigue testing done by Naidu and Raman (2005), applied slip displacement is prescribed via the applied cyclic stress. Applied stress is proportional to strain ($\sigma = E\varepsilon$), and strain is proportional to the change in gauge length ($\varepsilon = \Delta L/L$). When a fretting pad is applied to the elongating bar, interfacial slip, λ, will also be proportional to ΔL. Therefore, the induced slip displacement is proportional to applied cyclic stress. Thus variations in the friction coefficient observed by Naidu and Raman (2005) as a function of cyclic stress can be similarly related to changes in λ. This approach is taken by Siddiq and Ghassemieh's (2008) in their UC study to determine μ as a function of weld amplitude, λ. The third input parameter, weld speed, s, is inversely proportional to N, the number of cycles as shown in Eq. (3). In summary, F is proportional to contact pressure, λ is proportional to cyclic stress, and s is inversely proportional to N.

The empirical trends of Naidu and Raman's testing as related to the effect of contact pressure, cyclic stress, and N on μ is presented in Fig. 2 for reference. In 2007 Zhang and Li submitted a conference paper detailing an earlier version of their numerical model of the UC process. Part of this work included investigating the influence of temperature on the sliding friction coefficient of self mated Al. In Fig. 2 the data from Zhang and Li's (2007) study on μ vs. T is presented for reference.

Through inference the influence of λ, F, and s is not insignificant. As a result, a single valued constant friction coefficient, $\mu_{constant}$, may not be sufficiently accurate in predicting the heat generated during the process. Therefore, a coefficient of friction, μ_{RSM}, which depends on λ, F, and s, will also be investigated. This work will explore this dependence and compare the error introduced due to use of a constant friction coefficient.

2. Thermal friction model

Two different models for predicting the processing temperature during UC will be employed in this study. Both utilize the same heat flux term based on frictional work. However, the first model is analytic and spatially invariant, the other is a numerical finite element analysis (FEA) two-dimensional model. While the FEA solution is more detailed and can account for spatial variations, it requires

Please cite this article in press as: Koellhoffer, S., et al., Role of friction on the thermal development in ultrasonically consolidated aluminum foils and composites. J. Mater. Process. Tech. (2011), doi:10.1016/j.jmatprotec.2011.06.011

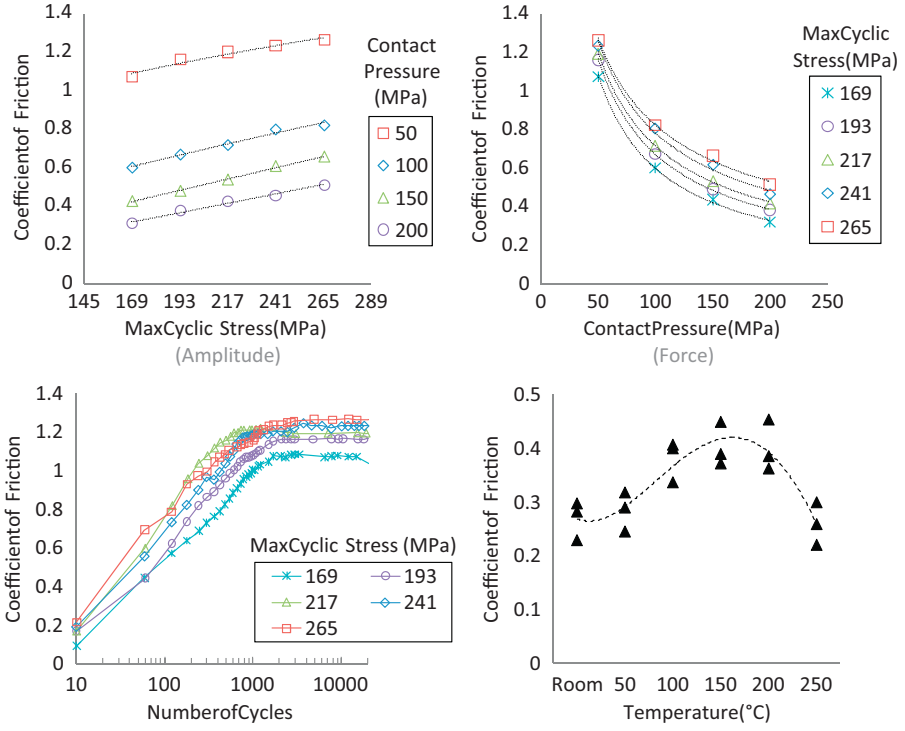

Fig. 2. Top and lower left, Naidu and Raman's (2005) friction trends as determined through uniaxial cyclic fretting fatigue testing. Lower right, Zhang and Li (2007) experimental μ vs. T results for Al–Al sliding contact [plots reproduced with permission].

more time to obtain results than the analytical solution. Therefore, if sample properties allow (e.g. low Biot's number; high internal conduction, and low convective loss, h, and small sample size, l), the analytic approach may be more appealing in an environment where FEA software is not easily utilized. This is further explained in Section 2.2.

2.1. Frictional heat generation term

Friction is a non-conservative force. Assuming all work done by friction is dissipated as heat over the contact area forms the basis of the friction model. The rate at which work is done (i.e. power) is the product of the force of friction and the average oscillatory speed, $\bar{v}$. Dividing the friction power by the contact area, $w \cdot l_c$, defines the frictional heat flux. This frictional flux can be written as:

$$q''_{fr} = \frac{F_{fr}\bar{v}}{wl_c} \tag{5}$$

The average oscillatory speed is dependent on frequency, f, and amplitude. Modeling the oscillatory motion, Λ, as a sinusoidal wave results in Eq. (6).

$$\Lambda = \frac{\lambda}{2} \sin 2\pi ft \tag{6}$$

Differentiating Λ with respect to time, t, yields the velocity. The average oscillatory speed is the average magnitude of the velocity. This is determined by integrating the absolute value of velocity over one period and multiplying it by the frequency. The resulting expression is:

$$\bar{v} = \overline{\left|\frac{d\Lambda}{dt}\right|} = 2\lambda f \tag{7}$$

By combining Eqs. (4), (5) and (7) with $F_N = F$, the horn applied clamping force, the frictional heat generation flux can be written as:

$$q''_{fr} = \frac{\mu F 2\lambda f}{wl_c} \tag{8}$$

2.2. Model implementation

The energy balance applied to the region of interest will allow one to solve for the temperature field as a function of time and position. The friction is generated at the interface so it can be introduced as a flux boundary condition. Before we embark on solving the three dimensional time dependent problem, it may be worthwhile to check if one can simplify the problem to just time dependent by evaluating the Biot number. When the Biot number is much less than one, there is usually not much of temperature gradient in the domain of interest and one can use lumped parameter analysis and solve analytically for the temperature as a function of time. In Incropera and DeWitt's (2001) introductory heat transfer textbook the Biot number is defined as:

$$Bi = \frac{hl}{k} \tag{9}$$

The Biot number is the ratio of convective losses to internal conduction. When materials are thin (small l) or highly conductive (large k), the internal temperature variation is small. Thus, for $Bi < 0.1$ (thermally thin) Incropera and DeWitt (2001) state that a material's internal temperature can usually be assumed to be spatially invariant making analytic temperature solutions possible. Conversely, thick samples with low conductivity and large convective losses will have spatially variant temperatures (thermally thick), which in turn are more involved to solve analytically. The Biot number is about 0.04 for welded foils and 0.08 for an MMC tape welded to an Al substrate. Both tape and foils have low Biot's numbers, but since foils and tapes have high aspect numbers (i.e. the ratio of cross-sectional length to thickness), the amount of

Please cite this article in press as: Koellhoffer, S., et al., Role of friction on the thermal development in ultrasonically consolidated aluminum foils and composites. J. Mater. Process. Tech. (2011), doi:10.1016/j.jmatprotec.2011.06.011

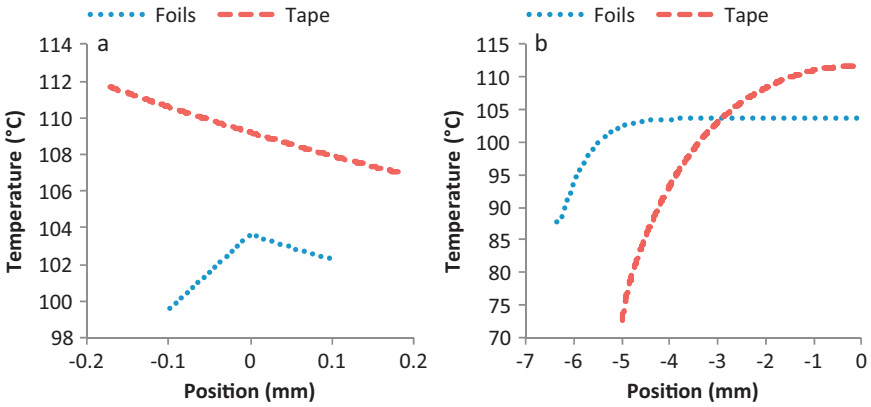

Fig. 3. Temperature variation for a typical weld: (a) through the tape's/foils' thickness at the midplane, (b) across the width (from the sample's edge to the midplane) at the weld interface. Note scale differences for temperature and position for each plot.

thermal variation in both the thru thickness direction and across the width at the weld interface should be investigated. Using the finite element analysis approach detailed later, the following plots were generated illustrating the amount of temperature variation for a typical weld through the tape's/foils' thickness at the midplane, Fig. 3(a), and across the width (from the sample's edge to the midplane) at the weld interface, Fig. 3(b). The average interfacial temperature for the tape and foils is the same, 102 °C.

In the thickness direction both foils and tapes show little variation in temperature. The coefficient of variation (CV) is 1% for foils and MMC tape. However, across the width larger variations are observed. The CV across the width is 3% for foils and 10% for tape. Therefore, the foils used in this study will be considered thermally thin, whereas the MMC tapes are thermally thick. Therefore, the solution approach will differ depending on the materials being consolidated. Foil temperatures will be solved using lumped parameter analysis, while tape temperatures will be predicted with a commercial FEA software package, COMSOL Multiphysics (2008).

2.2.1. Lumped parameter analysis

Since the temperature of welded foils does not vary spatially, temperature in the foil changes only with time. The first step is to perform an energy balance over the control volume of interest, the foil contact area and thickness. Any energy put into the control volume that is not dissipated into the surroundings is stored as described in Eq. (10).

$$\dot{E}_{in} - \dot{E}_{out} = \dot{E}_{stored} = \rho C_p V \frac{dT}{dt} \tag{10}$$

Fig. 4 illustrates the control volume for two identical foils being welded together. Thermal losses into the air, horn, and supporting anvil (flat knurled surface that secures the lower foil preventing slip during UC) are noted with outward arrows. The center shaded area represents the friction heat flux, q''_{fr}, which is the heat input into the control volume.

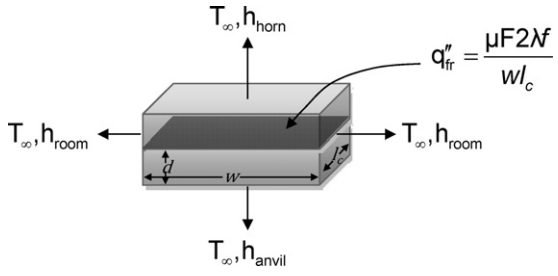

Fig. 4. Foil–foil control volume and thermal boundary conditions.

Using Eq. (10) in conjunction with the thermal loads from Fig. 4 the following equation is obtained:

$$\rho C_p V \frac{dT}{dt} = \dot{E}_{in} - \dot{E}_{out} = q''_{fr} \cdot wl_c - (h_{room} 4dl_c + h_{horn} wl_c + h_{anvil} wl_c) \times (T - T_\infty) \tag{11}$$

By assuming μ and the convection coefficients are independent of temperature and time, Eq. (11), which is a first order ODE, can be integrated to yield

$$T - T_\infty + \frac{\mu F 2\lambda f}{H(1 - e^{(-Ht/\rho C_p V)})} \tag{12}$$

where the volume, V; time, t; and equivalent convective losses, H; are given by:

$$V = 2dwl_c \tag{13}$$

$$t = \frac{l_c}{s} \tag{14}$$

$$H = (h_{room} 4dl_c + h_{horn} wl_c + h_{anvil} wl_c) \tag{15}$$

While losses to air, h_{room}, can be prescribed based on typical metal-to-still air values, h_{horn} and h_{anvil} cannot be predetermined. Thus, H is found empirically through inverse modeling using a two-dimensional FEA model and Eq. (12). This allows conductive losses to be effectively converted into a convective loss term. The resulting values for H are between 3.2 and 3.9 W/K depending on the total weld time. Since convective coefficients were assumed to be independent of time during integration, solutions to Eq. (12) will be slightly off. For the purpose of this study this is inconsequential since the temperature at the end of the weld is what will be predicted and measured.

2.2.2. Finite element analysis

The FEA analysis does not provide the level of insight of an analytic solution, but fewer assumptions are required, complicated geometries can be modeled, and graphical representation of results can be easily obtained. It is applied to the MMC tape as the Biot's number is close to 0.1 and it was shown that there is spatial variation in the temperature field (Fig. 3(b)). Fig. 5 shows the through-thickness two-dimensional FEA model: the boundary conditions, mesh properties, and heat flux boundary condition. Due to the confined space between the horn and substrate a low convective loss was assumed, $h = 5$ W/m^2 K, and applied on the dashed boundaries. The initial temperature is taken as ambient temperature, T_∞. A reduced half-symmetry geometry was used to minimize computational resources, while still being large enough

Please cite this article in press as: Koellhoffer, S., et al., Role of friction on the thermal development in ultrasonically consolidated aluminum foils and composites. J. Mater. Process. Tech. (2011), doi:10.1016/j.jmatprotec.2011.06.011

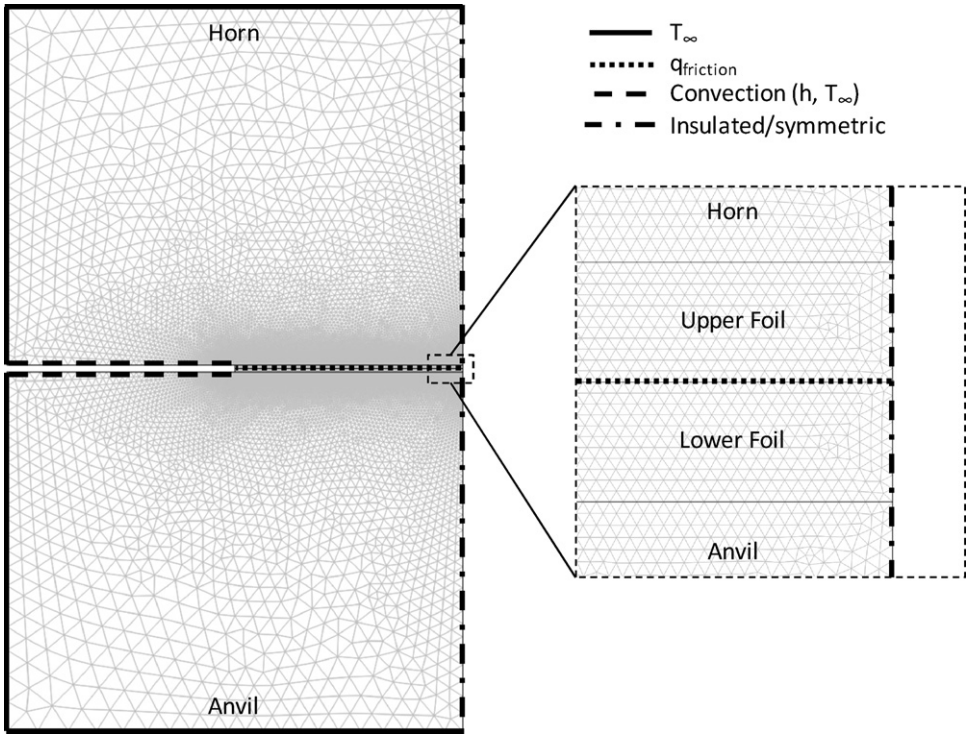

Fig. 5. FEA half-symmetry foil–foil model.

that thermal gradients are zero on the fixed temperature boundaries (indicated by a bold line). Mesh refinement was performed to assure convergence. For the tape–substrate FEA model a single tape replaces the foils, a substrate replaces the anvil, and q''_{fr} is applied at the tape–substrate interface. We can solve for temperature as a function of time in the entire domain.

3. Equipment, materials and experiments

In this section relevant laboratory equipment will be discussed. The geometric and thermal properties of the materials used will also be specified. All sample preparation and testing methods are detailed. The parameter selection criteria and parameter arrays are defined. And the process for obtaining the friction coefficient is explained.

3.1. Equipment

The primary equipment used in the study was an infrared camera and a customized ultrasonic welder. The infrared camera is used to measure temperature during the consolidation process. The ultrasonic welder is used to consolidate an MMC tape or metallic foil to a metal substrate or another foil.

3.1.1. Infrared camera

Heat given off by objects can be seen in the infrared (IR) spectrum. To measure the processing temperature of foils and tapes a FLIR Thermovision Alert, model 194, IR camera was used. The camera was mounted in front of the welder at a fixed distance/angle, and focused on the nip point between the horn and tape (or foil). Temperature dependent emissivities were calibrated using the same surrounding geometries and camera positioning on a hotplate. Fig. 6 shows the welding direction, overlaid IR image, temperature contours acquired (across the tape width), and camera positioning. The camera recorded in real time during the welding process. Each temperature contour captured corresponds to the temperature profile of the nip point from a single camera frame. This temperature profile is that of the sample just as welding is completed.

3.1.2. Ultrasonic welder

The welds were made with a modified seam welder purchased from AmTech. The knurled Ti–6Al–4V horn has a diameter of 146 mm, and can rotate at speeds up to 150 rpm resulting in weld speeds up to 1200 mm/s, via Eq. (1). The prescribed amplitude of oscillation and fixed frequency are regulated using feedback control built into the welder. The frequency used, 20 kHz, is, as reported by Neppiras' (1965) investigation of the physical mechanisms involved in ultrasonic welding, typical to ultrasonic welding. The clamping force is controlled with a pressure regulated pneumatic cylinder. The available parameter ranges (Table 2) for the welder are quite broad. This allows for greater flexibility and understanding of current and future welding geometries and material pairings. Depending on materials consolidated (foil–foil vs. tape–substrate) contact lengths, l_c, varied (see Table 1). From Askeland and Phulé's (2003) material science and engineering textbook it can be gathered that this is because the matrix metal in the MMC tape is pure Al, which has a yield strength 8–16 times lower than the foils,

Table 1
Material properties.

	Material	l_c (mm)	w (mm)	d (mm)	C_p (J/kg K)	k (W/m K)	ρ (kg/m^3)
Foil	Al 6061-T6	2.55	12.7	0.1	896	167	2700
Substrate	Al 6061-T6	7.22	25.4	12.7	896	167	2700
Tape	Al/Al_2O_3 (57% FVF)	7.22	10	0.36	802	81	3388

Please cite this article in press as: Koellhoffer, S., et al., Role of friction on the thermal development in ultrasonically consolidated aluminum foils and composites. J. Mater. Process. Tech. (2011), doi:10.1016/j.jmatprotec.2011.06.011

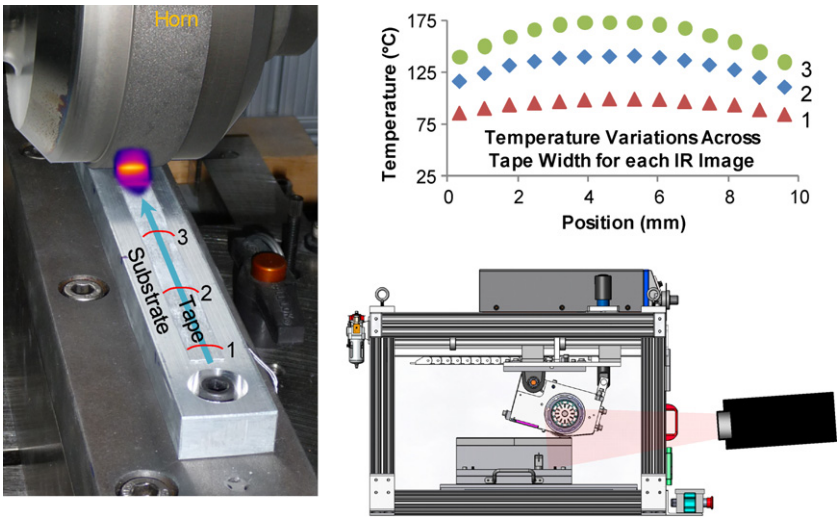

Fig. 6. IR camera positioning and acquired data.

Table 2
Current welder parameter ranges.

	Available parameter range
Amplitude (μm)	6–45
Force (N)	300–5500
Speed (mm/s)	0–1200

17–34 MPa vs. 276 MPa. A lower yield strength means that a larger amount of contact area is needed to support the same load. Additional detail regarding the contact length and the procedure for determining l_c will be discussed further in Section 3.3.1.

3.2. Materials

The foils and substrates used in this study were aluminum alloy 6061 heat treated to the T6 condition. The Askeland and Phulé (2003) textbook reports that the T6 temper designation indicates the material has been solution treated and artificially aged to strengthen it. The foils in this study were heat treated in an oxygenated environment resulting in a very thick oxide layer. This layer can be removed with a low concentration nitric acid bath (3% for 18 h). Foils treated with nitric acid will be referred to as *cleaned* foils. Untreated foils will be referred to as *oxidized* foils. This step was not necessary for substrate welding as no thick oxide existed; implying that, unlike the foils, the heat treatment process was performed in a more inert environment. The MMC tapes were provided by the Army Research Laboratory. The tapes, commercially known as MetPreg, were fabricated by Touchstone Research Laboratory (TRL). MetPreg consists of Nextel 610 alumina fibers in a pure aluminum matrix. The roll used in this study was 57% fiber volume fraction (FVF). Micrographs of a cross-section of MetPreg are shown in Fig. 7. There is a large amount of variation in thickness from the edge (0.43 mm) of the specimen to the center (0.32 mm), 30% difference. After UC tape thickness, and variation, is reduced (−8%), and width increases (+9%). For thermal modeling the tape geometry was held constant and assumed rectangular; an in situ geometry was used that consisted of an average of pre and post-processed measured tape dimensions (Table 1). Foils on the other hand had no measureable variation in thickness or width, pre or post UC. Unlike the pure Al matrix of the MMC tape, the high yield strength of Al 6061-T6 is more resistant to plastic deformation. Thus for foils the model geometry was also the pre and post weld measured thickness and width. The fact that the MMC tape deforms during UC will not significantly affect the thermal development, since deformational contributions are expected to be on the order of 1%, as indicated in Section 1.1. Geometric and thermal properties for all consolidated samples are summarized in Table 1.

3.3. Experiments

The primary goal of the experiments is to record the temperature of the foil or tape during the UC process. This temperature is then compared to the values predicted from the model based on the best-fit value for a single valued constant friction coefficient, $\mu_{constant}$, and for a coefficient of friction, μ_{RSM}, that is allowed to vary with the machine variables. Once μ is known, a subsequent test array, or validation experiment, is performed to assess the accuracy of the model proposed. Both oxidized and cleaned foils were subjected to UC. Oxidized foils are not expected to bond while cleaned foils are. This is due to the thick oxide layer present. The bonding process relies on the breakup of the oxide layer to produce clean metal surfaces that provide paths of diffusion. In Janaki Ram et al.'s (2007) work of UC of multi-material systems it is discussed that if the oxide is not broken apart and properly dispersed voids will remain since the UC bonding process is relies on metal–metal contact. Thus welds using oxidized foils will be representative of pure slip, friction only condition. Inconsistencies in friction coefficient trends between oxidized and cleaned foils can, in part, be attributed to potential deformational heating effects, which are expected to be small. All foils are consolidated using a foil–foil setup as shown in Fig. 8. In this arrangement, both the horn and anvil contacting surfaces are knurled to prevent foil slip at the tool–foil interfaces.

For MMC tape welds, a tape–tape geometry was not used. Stacking two unprocessed tapes on top of each other amplifies the tape's geometric non-uniformities resulting in non-uniform temperatures. Fig. 9 illustrates the difference in temperature distributions across the sample's width of a tape–tape and tape–substrate weld. The samples compared have similar (4% difference) average temperatures, but substantially different process settings. Weld settings for force, speed, and amplitude were: 1451 N, 51.3 mm/s, and 28.4 μm for the tape–tape weld and 2461 N, 19.3 mm/s, and 25.8 μm for the tape–substrate weld, respectively. While sufficient energy can be delivered to permit gap closure of a tape–tape sample; this resulted in tool sticking at the anvil–tape interface. By welding to a substrate (Fig. 8(b)), energy levels can be increased and non-uniformities are greatly reduced. Note that for tape–substrate welds a knurled anvil is not used to prevent slip, instead the substrate is bolted in place (as shown in Fig. 6).

Please cite this article in press as: Koellhoffer, S., et al., Role of friction on the thermal development in ultrasonically consolidated aluminum foils and composites. J. Mater. Process. Tech. (2011), doi:10.1016/j.jmatprotec.2011.06.011

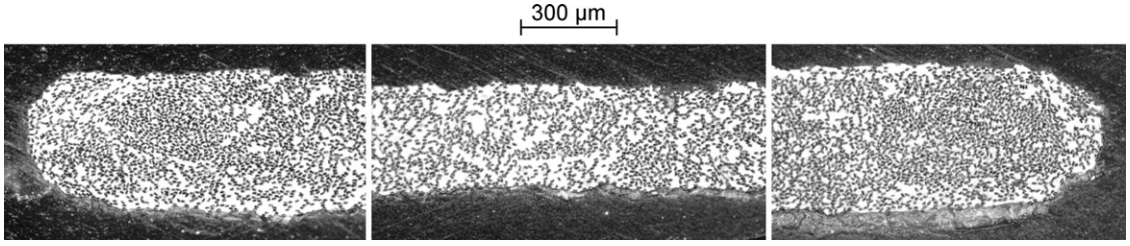

Fig. 7. Optical microscope images of a through thickness cross-section of MetPreg. Images show left center and right views.

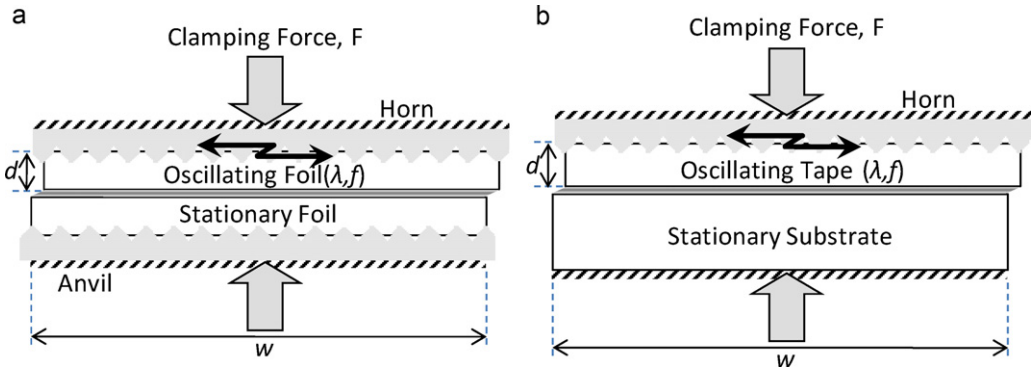

Fig. 8. Welding geometries: (a) foil–foil with knurled anvil; (b) tape–substrate with bolt down substrate.

3.3.1. Contact length, l_c

The contact length between materials to be consolidated was determined by performing a series of *spot* welds over a range of pressures. Spot welds were performed by welding a sample with a feed rate of 0 mm/s and amplitude of 24 μm for a duration of approximately 0.2 s. Upon separation of consolidated samples the length over which friction abraded the contacting surfaces is measured and defined to be the contact length. The abraded area was slightly larger than the previously bonded areas. This prevented any potential bias that could have occurred should tearing of the bonded region take place. Neither foil–foil welds nor tape–substrate bonds showed significant dependence on pressure (see Fig. 10). That is to say, the apparent contact area did not depend on pressure; however, the real contact area will be influenced by the applied load since the sample's surface will deform until enough area is in contact to balance the applied load. The variation in real contact area will alter the contact geometry which, according to Blau's (2009) well documented book on friction concepts and applications, is known to affect the friction coefficient, which may be one of the reasons force can influence μ. For this model, apparent area is used, so variation in real contact area is not quantified. For foils and tapes the average contact lengths were 2.55 and 7.22 mm, respectively. The longer contact length between the tape and the substrate can be attributed to several factors including: narrower tape width, greater thickness, and softer base metal.

3.3.2. Friction coefficient determination

For foils, Eq. (12) can be solved explicitly for μ as a function of temperature. For tapes, μ must be found iteratively from inverse modeling. With a 16 sample test array, the end result for both foils and tapes is a series of 16, likely different, friction coefficients; one for each weld. These values are averaged if one wants to report a single value, $\mu_{constant}$, or further analysis is carried out to determine a parameter dependent function, μ_{RSM}.

To determine $\mu_{constant}$ all 16 values were averaged. This results in the single valued constant friction coefficient, $\mu_{constant}$, which is valid over the range of processing parameters tested. To find μ_{RSM} a response surface model (RSM) was generated which fits a surface to the experimentally determined friction coefficients. This is done by fitting a quadratic equation, which includes all linear combinations

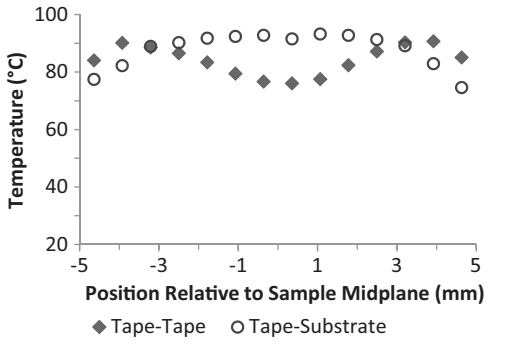

Fig. 9. Comparison of temperature uniformity across the width of a tape–tape weld and a tape–substrate weld.

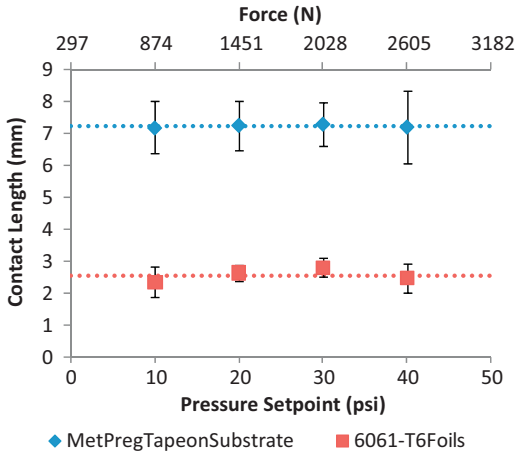

Fig. 10. Contact length between consolidated materials as a function of applied load.

of parameters according to a second order polynomial, Eq. (16), to the experimental data.

$$\mu_{RSM} = b_0 + b_\lambda\tilde{\lambda} + b_F\tilde{F} + b_s\tilde{s} + b_{\lambda\lambda}\tilde{\lambda}^2 + b_{FF}\tilde{F}^2 + b_{ss}\tilde{s}^2 + b_{\lambda F}\tilde{\lambda}\tilde{F} + b_{\lambda s}\tilde{\lambda}\tilde{s} + b_{Fs}\tilde{F}\tilde{s} \quad (16)$$

where the b's are the fitting coefficients and $\tilde{\lambda}$, $\tilde{F}$, and $\tilde{s}$ are coded welder parameters; all of which are dimensionless. Coded parameters vary between −1 and 1 taking the form:

$$\tilde{x} = \frac{x - x_{avg}}{\Delta x} \quad (17)$$

$$\Delta x = \frac{x_{\max} - x_{\min}}{2} \quad (18)$$

The credibility of μ, constant or variable, is assessed by comparing the trends in μ determined from the experiments to the expected trends from the literature, Fig. 2. Once the coefficient of friction is known a new test array was created to evaluate the model's accuracy.

3.3.3. Parameter selection

The selection process for welder parameters differed for foils and tapes. To minimize the effects of deformation, oxidized foils were given the maximum amount of energy that did not result in welding, thus allowing for pure slip throughout the welding process. The same parameter array was employed for cleaned foils to allow for comparison. The oxide layer is much thinner for cleaned foils, so bonding did occur during consolidation. Therefore, cleaned foils may not slip throughout the entire weld duration. The modifications in surface characteristics will alter the frictional behavior. Blau's (2009) book reports that surface oxide presence has a lubricating effect, reducing μ. Therefore, increases in μ can be attributed to the pretreatment acid removal of *lubricating* surface oxides. Variations in μ may also result from bonding/no-slip deformational influences. While the additive contribution of deformational heat is small, the prevention of slip could result in less frictional heat generation; if this is the case the apparent μ (i.e. the μ calculated with this approach) will be smaller than the real μ at regions experiencing slip.

Tape welding parameters were chosen to achieve good bonding and uniform heating. A good bond is one in which the tape, or foil, breaks in tension or flexure prior to fully debonding from its mating surface. This test is performed qualitatively. To date there is not an established testing method that can fully characterize the bond strength between UC materials; though, an extensive body of work on mechanical testing of ultrasonically consolidated thin foils has been performed at Loughborough University. In 2003 Kong et al. began their method development of mechanical testing of UC Al 6061 welds. In 2004(a) Kong et al. continued their work with Al 3003; methods such as lap-shear and peel test have been attempted; however typical failure modes do not occur uniformly in the bonded interface. Samples either break outside of the bonded region, or tear non-uniformly failing to capture the stable debonding load. Nevertheless, the peel test is the most commonly used method in Loughborough's work and was recently employed in Friel et al.'s (2010) paper to investigate the effect of surface topography for UC of Al.

Uniform heating is characterized by removal of the thermal edge peaks, or double peaks, shown in Fig. 9. As load levels increase, pressure in particular, greater levels of uniformity are achieved. Due to the thermal mass of the horn and substrate, edge effects cannot be completely eliminated.

The corresponding parameter ranges found to fit the desired welding criterion specified in this section are summarized in Table 3. Note that tape–substrate welds used higher levels of all parameters than foil–foil welds. This was necessary to achieve uniform heating.

Table 3
Experimental parameter ranges used during UC.

	Foil–foil	Tape–substrate
Amplitude (μm)	9.4–18.4	24–34
Force (N)	874–1739	1739–2605
Speed (mm/s)	87–123	10–56

Table 4
Initial L16 Taguchi array.

Sample #	Amplitude (μm)		Force (N)		Speed (mm/s)	
	Foils	Tape	Foils	Tape	Foils	Tape
1	9.4	34.0	1162	2028	99.2	25.4
2	12.4	24.0	874	1739	99.2	56.2
3	18.4	27.3	1739	2028	87.2	56.2
4	12.4	27.3	1451	1739	123	40.8
5	9.4	34.0	874	1739	87.2	10.1
6	15.4	24.0	874	2317	111	25.4
7	9.4	27.3	1451	2605	111	25.4
8	15.4	30.7	1451	2028	87.2	10.1
9	15.4	24.0	1162	2605	123	10.1
10	18.4	34.0	1162	2605	111	56.2
11	12.4	30.7	1739	1739	111	25.4
12	18.4	24.0	1451	2028	99.2	40.8
13	12.4	27.3	1162	2317	87.2	10.1
14	9.4	34.0	1739	2317	123	40.8
15	18.4	30.7	874	2317	123	56.2
16	15.4	30.7	1739	2605	99.2	40.8

3.3.4. Parameter implementation

A design of experiments approach was taken to generate the UC test array. Design of experiments is a method often used to optimize or predict a system response, in this case temperature. A four level L16 orthogonal Taguchi array was first employed to determine the friction coefficient by means of the processing temperature. A subsequent 3-by-3 test array was then used to assess the model's temperature prediction accuracy and limitations. The L16 and 3-by-3 arrays used for the foil–foil tests and the tape–substrate test were run according to the sequences shown in Tables 4 and 5, respectively.

4. Results and discussion

The thermal results from the initial test array and the resulting calculated friction coefficients are presented in this section. An analysis of the experimentally determined friction coefficients is detailed by comparing calculated and literature values. A subsequent validation test using the determined friction coefficients is executed to indicate the model's accuracy.

Table 5
Validation (3-by-3) array.

Sample #	Amplitude (μm)		Force (N)		Speed (mm/s)	
	Foils	Tape	Foils	Tape	Foils	Tape
1	16.9	32.5	1595	2172	111	50.0
2	16.9	25.8	1018	1884	99.2	50.0
3	13.9	25.8	1018	2461	111	19.3
4	16.9	29.1	1307	2461	87.2	34.7
5	13.9	32.5	1307	1884	87.2	19.3
6	10.9	32.5	1018	2461	123	50.0
7	13.9	29.1	1595	1884	123	34.7
8	10.9	29.1	1307	2172	99.2	34.7
9	10.9	25.8	1595	2172	87.2	19.3

Please cite this article in press as: Koellhoffer, S., et al., Role of friction on the thermal development in ultrasonically consolidated aluminum foils and composites. J. Mater. Process. Tech. (2011), doi:10.1016/j.jmatprotec.2011.06.011

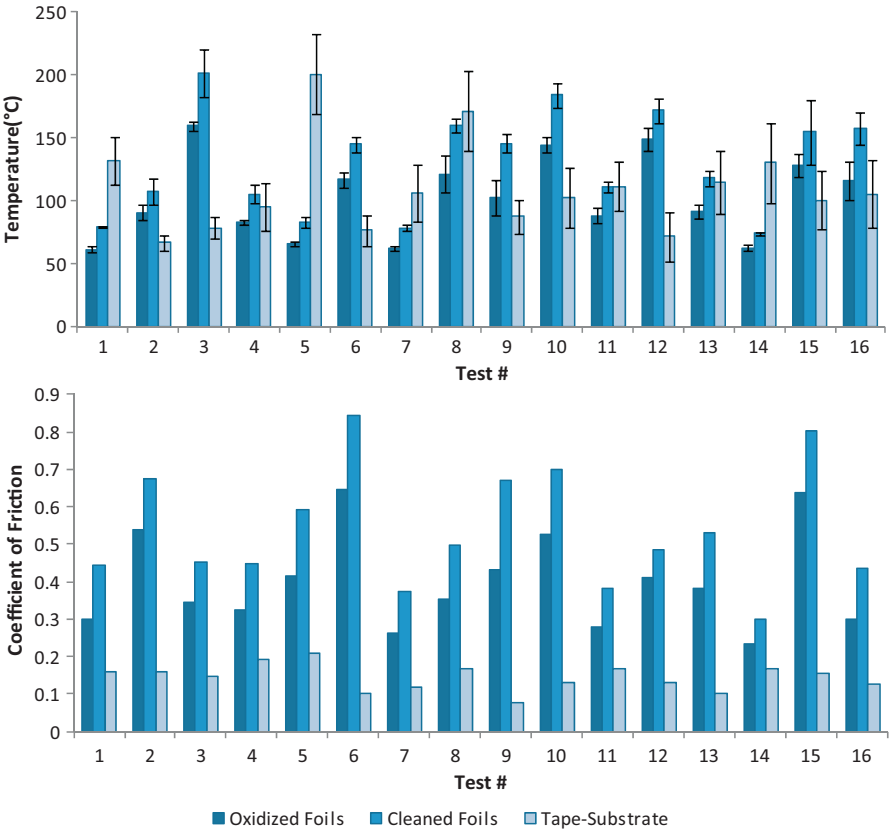

Fig. 11. L16 Results – Temperature (top) and friction coefficients (bottom).

4.1. L16 array – temperature and friction coefficient results

The temperature results and calculated friction coefficients from the initial L16 array are shown in Fig. 11. Sample numbers from Table 4 correspond to the test numbers in Fig. 11. Tape–substrate temperatures were obtained by averaging all temperature contours in the length and width direction. Foil temperatures were obtained by averaging the maximum temperature recorded for each contour. Maximum temperature was used for foils because it is less computationally intensive to obtain. Since the Biot number of the foils is low (i.e. temperature is spatially invariant), maximum and average temperatures are comparable. As expected there is a large amount of variability among the computed friction coefficients. A summary of friction values obtained is shown in Table 6. The range of results determined in this study fall within the same range as reported in the literature (see Fig. 2).

The friction coefficient for tape–substrate welding is substantially lower than that of the foil–foil. This is a result of differing loading conditions and material properties. For foil–foil welds, loads were chosen specifically to avoid plastic deformation. However, this was not the case for the MetPreg tape–substrate welds. For tape welds the normal load alone was in excess of the matrix material's room temperature yield strength. Additionally, changes to the tapes cross-sectional area post-welding also support the presence of bulk plastic deformation during consolidation. Bhushan's (1999) comprehensive textbook on tribology presents a preliminary derivation for plastic contact of ductile metals which suggests $\mu \leq 1/5$; this is much lower than typical sliding friction coefficients. This explains the decreased friction coefficient observed during UC of tapes.

Friction coefficients also differed when comparing oxidized and cleaned foils. Oxidized foils have a larger amount of aluminum oxide, Al_2O_3, present on the surface as compared to cleaned foils. Bhushan's (1999) textbook reports self-mated friction coefficient values for Al are higher than that of Al_2O_3. In addition to changing the surface oxidation levels, cleaning can remove trace lubricants and other contaminants. Blau's (2009) book describes that the more thorough the cleaning process, the higher the friction coefficient can become.

Another interesting observation is the amount of variation during testing for each material pairing. The coefficient of variation, CV, of measured temperatures, T-CV, was just over 30% for all material pairings. For foils, oxidized and cleaned, this correlated to a μ-CV of roughly 30%, while tape–substrate welds had a μ-CV of only 20%. Thus, the friction behavior of an ultrasonically consolidated tape–substrate interface is not as easily influenced by welder parameters as a foil–foil interface. This could be a function of the large difference in time scales. Weld times were on average more than 10 times longer for tapes than foils. Thus it is more likely for the friction coefficient to have fully stabilized (Fig. 2, μ vs. N). Fiber reinforcement may also play a role by affecting the abrasion resistance of the contacting surfaces. By limiting wear, the surface properties could be less susceptible to external forces (i.e. welder parameter settings). An investigation into the wear mechanics of UC materials may provide more insight into this phenomenon.

Table 6
L16 friction coefficients.

	Average	Minimum	Maximum	Coefficient of variation
Oxidized foils	0.399	0.233	0.644	32%
Cleaned foils	0.539	0.301	0.843	29%
Tape–substrate	0.145	0.076	0.211	24%

Please cite this article in press as: Koellhoffer, S., et al., Role of friction on the thermal development in ultrasonically consolidated aluminum foils and composites. J. Mater. Process. Tech. (2011), doi:10.1016/j.jmatprotec.2011.06.011

Table 7
μ_{RSM} – response surface model coefficients.

	b_0	b_λ	b_F	b_s	$b_{\lambda\lambda}$	b_{FF}	b_{ss}	$b_{\lambda F}$	$b_{\lambda s}$	b_{Fs}
Oxidized foils	0.3885	0.0952	−0.1547	0.0015	−0.0173	0.0561	−0.0201	−0.0326	−0.0383	0.0129
Cleaned foils	0.5430	0.0897	−0.1771	0.0221	−0.0470	0.0464	−0.0067	−0.0082	−0.0094	−0.0122
Tape–substrate	0.1462	0.0238	−0.0269	0.0087	−0.0077	0.0067	−0.0018	−0.0040	−0.0119	0.0018

4.1.1. Variable friction coefficient – RSM

Minitab (2003) was used to perform the response surface model calculation as described in the experimental section. The RSM coefficients are shown in Table 7. The values from Table 7 can then be paired with Eq. (16) to plot the trends of the friction coefficient for each material pairing over a range of amplitudes, forces, and speeds (Figs. 12–14).

4.2. Friction coefficient validity

There is good correlation in the coefficient of friction trends when comparing the experimental results here (Figs. 12–14) to fretting fatigue experiments done by Naidu and Raman (2005), Fig. 2. In Figs. 12–14, L, M, and H correspond to Low, Medium, and High welder parameter levels, respectively. Low is the lowest setting tested experimentally, Medium is the average, and high is the highest. From Figs. 12–14, increase in oscillation amplitude causes an increase in μ, while normal force has a diminishing effect. This directly correlates to the literature findings. On the other hand speed, or number of cycles, N, has little effect on μ. Under isothermal conditions, speed should have no effect on μ, however, UC is not an isothermal process, and thus lower speeds (higher N) correspond to higher temperatures. This introduces the potential for error since μ does depend on temperature as illustrated by Zhang and Li's (2007) experimental results previously discussed, Fig. 2. As a result the friction coefficient for both foils and tapes exhibit some dependence on speed which may be attributable to this effect. Thus, assuming μ does not depend on temperature introduces a small amount of error.

Another potential source of error is the presence of deformational heating. This model assumes frictional heating only throughout the entire welding process. Thus, any deformational heating gets intrinsically lumped in to the friction coefficient. However, contributions from deformation are small (Section 1.1) and the μ trends across all material pairings are very similar suggesting the driving force behind the thermal development is also similar. When welding oxidized foils it was made certain that machine parameters were chosen so as to avoid effects from the deformational regime, in particular bonding. Thus, oxidized foils were welded under pure slip conditions, therefore friction dominant. Since trends in the friction coefficient from the friction dominated oxidized foil welds are similar for the other material pairings, this supports that friction is also the dominant heating mechanism for cleaned foils and tape–substrate welds.

4.3. Validation

With both $\mu_{constant}$ and μ_{RSM} characterized by minimizing the error between the predicted and experimental temperatures, a 3-by-3 array of the three distinct values of the three processing parameters (F, s and λ), as listed in Table 5, was executed experimentally and the values for the temperature field were recorded. The model was used with the characterized value of both $\mu_{constant}$ and μ_{RSM} to predict the temperatures and compare them to the experimental values. Predicted and experimental temperatures for each material pairing are shown in Fig. 15. Good agreement was achieved. A constant friction coefficient results in an error of 16% on average. While a parameter dependent friction coefficient reduces this error to 7%. The fitting error of the RSM is of the same order;

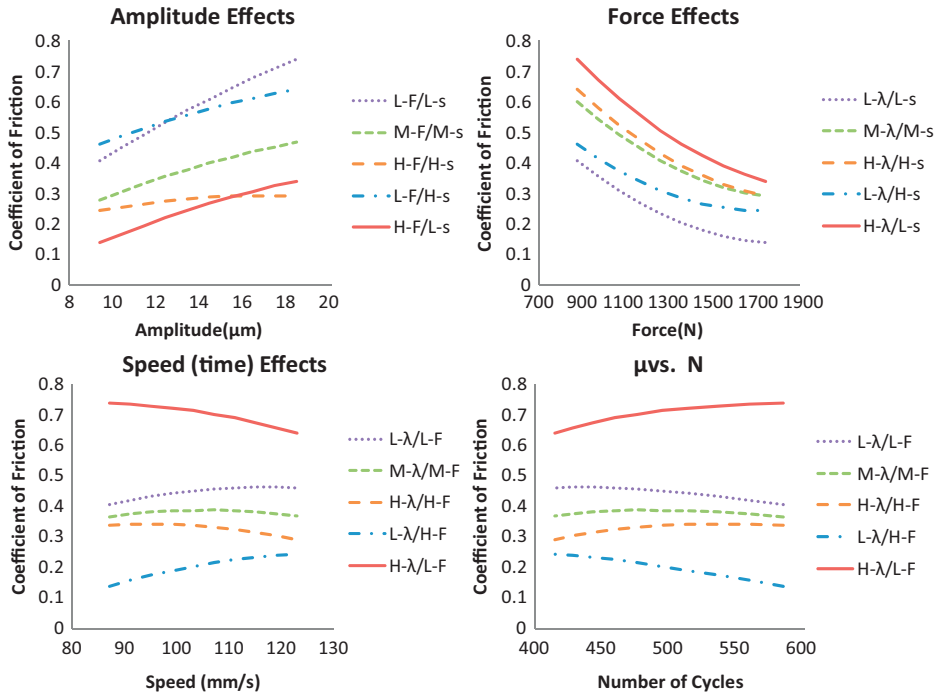

Fig. 12. Friction coefficient trends – oxidized foils – L, M, and H correspond to Low, Medium, and High welder parameter levels, respectively. Low is the lowest setting tested experimentally, Medium is the average, and High is the highest.

Please cite this article in press as: Koellhoffer, S., et al., Role of friction on the thermal development in ultrasonically consolidated aluminum foils and composites. J. Mater. Process. Tech. (2011), doi:10.1016/j.jmatprotec.2011.06.011

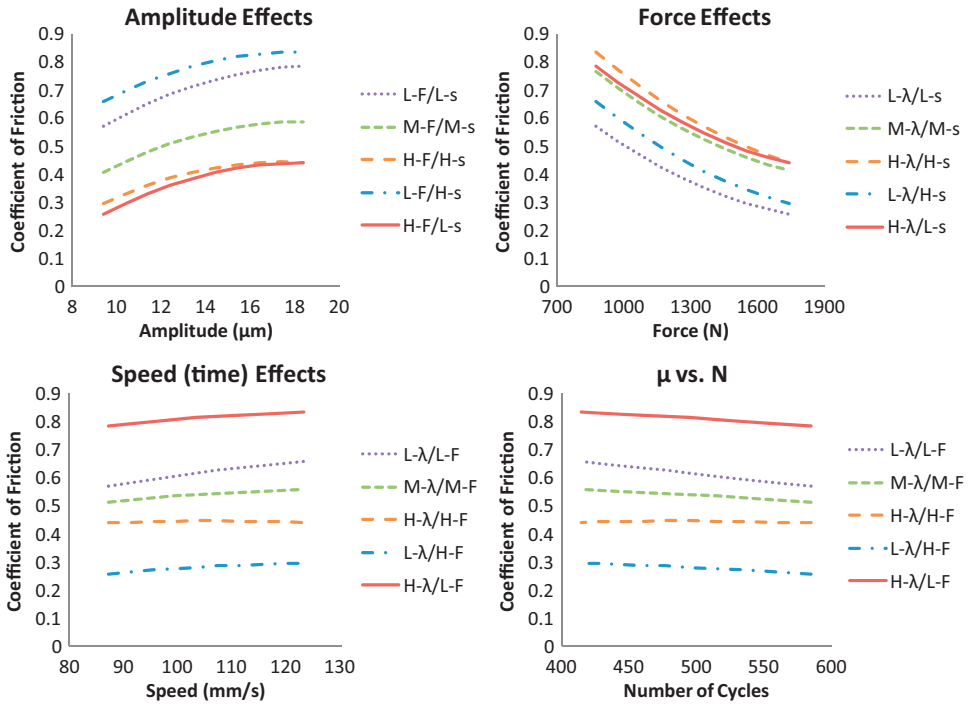

Fig. 13. Friction coefficient trends – cleaned foils – L, M, and H correspond to Low, Medium, and High welder parameter levels, respectively. Low is the lowest setting tested experimentally, Medium is the average, and High is the highest.

therefore, 7% error is very good agreement. The average, maximum and minimum error percentages are summarized in Table 8. While $\mu_{constant}$ did not result in a high average error, it did result in very high maximum error. The highest errors occurred when force and amplitude were out of phase with each other (i.e. one high, the other low). As with the L16 array used in Section 4.1, temperature is reduced to an average value for each test. This is the case for both measured and predicted values. For foil predictions this is the only option since a lumped parameter model was employed. For tape welds temperature contours can be plotted across the foil width,

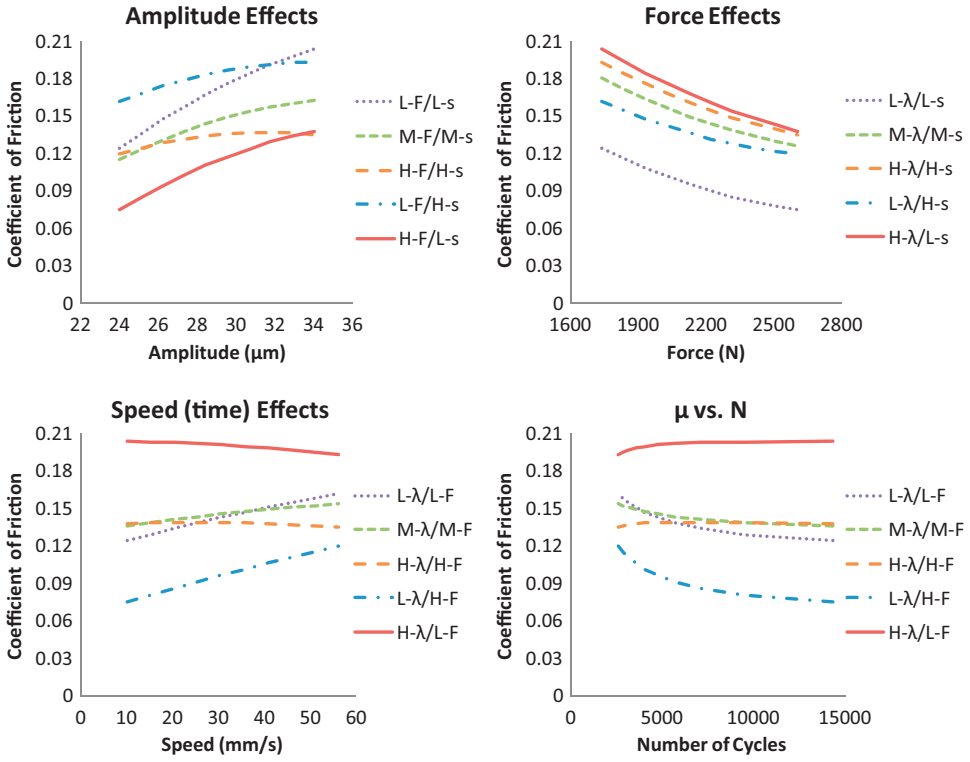

Fig. 14. Friction coefficient trends – tape on substrate – L, M, and H correspond to Low, Medium, and High welder parameter levels, respectively. Low is the lowest setting tested experimentally, Medium is the average, and High is the highest.

Please cite this article in press as: Koellhoffer, S., et al., Role of friction on the thermal development in ultrasonically consolidated aluminum foils and composites. J. Mater. Process. Tech. (2011), doi:10.1016/j.jmatprotec.2011.06.011

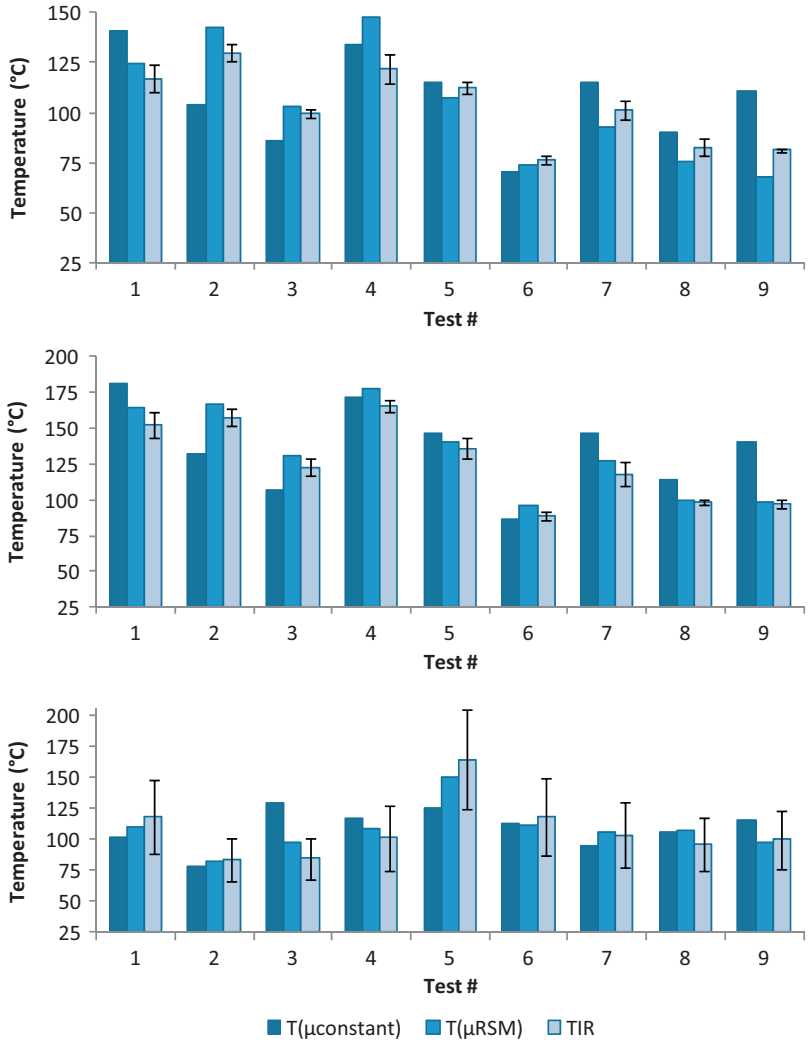

Fig. 15. Model validation array (3-by-3 array): top, oxidized foil–foil; middle, cleaned foil–foil; bottom, tape–substrate. T_{IR} is the experimentally measured average temperature (average maximum for foils and average of all data for tapes) with error bars indicating the size of the standard deviation, plus and minus. "$T(\mu_{constant})$" and "$T(\mu_{RSM})$" are the analytic (foils) or FEA (tape) temperature solutions using a constant and parameter dependent (RSM) friction coefficient, respectively.

Table 8
Model accuracy within the range of parameters in which the friction coefficient is characterized. Error between model and experiments reported in percentages.

	Oxidized foils		Cleaned foils		MetPreg L16-T (°C)	
	$T(\mu_{constant})$	$T(\mu_{RSM})$	$T(\mu_{constant})$	$T(\mu_{RSM})$	$T(\mu_{constant})$	$T(\mu_{RSM})$
Avg	15%	9%	16%	5%	17%	7%
Min	2%	4%	3%	1%	5%	2%
Max	36%	21%	46%	8%	52%	16%

and when plotted do follow a parabolic distribution similar to that of the measured data in Fig. 6. To facilitate quantitative comparisons the average temperature was used.

5. Conclusions

The processing temperature during ultrasonic consolidation of thin foils and prepreg metal matrix composite tapes can be predicted using a friction work heat generation model. Many factors can influence the magnitude of the friction coefficient. Surface condition is one such factor, oxidized vs. cleaned. Cleaned surfaces provide more sliding resistance than oxidized surfaces. Stress state also affects the amount of friction present; plastic deformation suppresses the friction coefficient. The friction coefficient can be taken to be either constant, or parameter dependent. However, literature and our experiments show significant dependence of the coefficient of friction on the machine parameters during ultrasonic consolidation. Model accuracy, in particular for unbalanced loads (i.e. high force, low amplitude), is much improved when using a parameter dependent friction coefficient. The model developed here can now be applied to other aspects of the ultrasonic consolidation process such as characterizing the thermo-mechanical response or bond strength and development.

Acknowledgement

We would like to thank the Army Research Laboratory (ARL) for support of this research and for funding through the Composite Materials Research program.

References

Askeland, Phulé, 2003. The Science and Engineering of Materials: Fourth Edition.
Bhushan, B., 1999. Principles and Applications of Tribology. John Wiley & Sons, Inc., New York.
Blau, P.J., 2009. Friction Sci. Technol..
Bowden, F.P., Tabor, D., 1950. The Friction and Lubrication of Solids. Clarendon Press, Oxford.

Cheng, X., Datta, A., Choi, H., Zhang, X., Li, X., 2007. Study on embedding and integration of micro sensors into metal structures for manufacturing applications. ASME J. Manuf. Sci. Eng. 129, 416–424.
Clews, J.D., 2009. Ultrasonic Consolidation of Continuous Fiber Metal Matrix Composite Tape. University of Delaware, Newark, DE, p. 190.
COMSOL, 2008. COMSOL Multiphysics: Version 3.5a. COMSOL AB, Stockholm, Sweden.
Doumanidis, C., Gao, Y., 2004. Mechanical modeling of ultrasonic welding. Weld. J. 83 (4), 140-s–146-s.
Friel, R.J., Johnson, K.E., Dickens, P.M., Harris, R.A., 2010. The effect of interface topography for ultrasonic consolidation of aluminium. Mater. Sci. Eng. A 507 (16–17), 4474–4483.
Gunduz, E., Ando, T., Shattuck, E., Wong, P.Y., Doumanidis, C.C., 2005. Enhanced diffusion and phase transformations during ultrasonic welding of zinc and aluminum. Scr. Mater. 52 (9.), 939–943.
Hazlett, T.H., Ambekar, S.M., 1970. Additional studies of interface temperature and bonding mechanisms of ultrasonic welds. Weld. J. 49 (5), 196-s–200-s.
Hibbeler, R.C., 2002. Mechanics of Materials, 5th ed. Prentice Hall, New Jersey.
Hodowany, J., 1997. On the conversion of plastic work into heat. California Institute of Technology. CaltechTHESIS, 118.
Incropera, F.P., DeWitt, D.P., 2001. Introduction to Heat Transfer, 4th ed. John Wiley & Sons, Inc., New York.
Janaki Ram, G.D., Robinson, C., Yang, Y., Stucker, B., 2007. Use of ultrasonic consolidation for fabrication of multi-material structures. Rapid Prototyp. J. 13 (4), 226–235.
Kong, C.Y., Soar, R.C., Dickens, P.M., 2003. Characterisation of aluminium alloy 6061 for the ultrasonic consolidation process. Mater. Sci. Eng. A 363 (1–2), 99–106.
Kong, C.Y., Soar, R.C., Dickens, P.M., 2004a. Optimum process parameters for ultrasonic consolidation of 3003 aluminum. J. Mater. Process. Technol. 146, 181–187.
Kong, C.Y., Soar, R.C., Dickens, P.M., 2004b. Ultrasonic consolidation for embedding SMA fibres within aluminium matrices. Composite Structures 66 (1–4), 421–427.
Kong, C.Y., Soar, R.C., 2005a. Fabrication of metal–matrix composites and adaptive composites using ultrasonic consolidation process. Mater. Sci. Eng. A 412 (1–2), 12–18.
Kong, C.Y., Soar, R.C., 2005b. Method for embedding optical fibres in an aluminium matrix by ultrasonic consolidation. Appl. Opt. 44, 6325–6333.
Langenecker, B., 1966. Effects of ultrasound on deformation characteristics of metals. IEEE Trans. Sonics Ultrasonics SU-13, 1–8.
Mariani, E., Ghassemieh, E., 2010. Microstructure evolution of 6061 O Al alloy during ultrasonic consolidation: an insight from electron backscatter diffraction. Acta Mater. 58, 2492–2503.
Minitab, 2003. Release 14. Minitab Inc., Pennsylvania.
Naidu, N.K., Raman, S., 2005. Effect of contact pressure on fretting fatigue behavior of Al–Mg–Si alloy AA 6061. Int. J. Fatigue 27, 283–291.
Neppiras, E.A., 1965. Ultrasonic welding of metals. Ultrasonics 3 (3), 128–135.
Ravichandran, G., Rosakis, A.J., Hodowany, J., Rosakis, P., Furnish, M.D., Thadhani, N.N., et al., 2002. On the conversion of plastic work into heat during high-strain-rate deformation. AIP Conf. Proc. 620 (1), 557–562.
Siggard, E.J., Madhusoodanan, A.S., Stucker, B., Eames, B., 2006. Structurally embedded electrical systems using ultrasonic consolidation (UC). In: Proceedings of the 17th Solid Freeform Fabrication Symposium , Austin, Texas, USA, August.
Siddiq, A., Ghassemieh, E., 2009. Theoretical and FE analysis of ultrasonic welding of aluminum alloy 3003. J. Manuf. Sci. Eng. 131 (4), 041007-1–041007-11.
Siddiq, A., Ghassemieh, E., 2008. Thermomechanical analyses of ultrasonic welding process using thermal and acoustic softening effects. Mech. Mater. 40 (12), 982–1000.
Tierney, J., Gillespie, J.W., 2006. Modeling of in situ strength development for the thermoplastic composite tow placement process. J. Compos. Mater. 40 (16), 1487–1506.
White, D.R., 2003. Ultrasonic consolidation of aluminum tooling. Adv. Mater. Processes 161 (1), 64–65.
Yang, Y., Janaki Ram, G.D., Stucker, B.E., 2009. Bond formation and fiber embedment during ultrasonic consolidation. J. Mater. Process. Technol. 209 (10), 4915–4924.
Zhang, C., Li, L., 2007. Effect of friction on ultrasonic consolidation. In: Proceedings of the 2007 International Manufacturing Science and Engineering Conference, ASME (paper number MSEC2007-31202).
Zhang, C., Li, L., 2009. A coupled thermal–mechanical analysis of ultrasonic bonding mechanism. Metall. Mater. Trans. B 40, 196–207.

Please cite this article in press as: Koellhoffer, S., et al., Role of friction on the thermal development in ultrasonically consolidated aluminum foils and composites. J. Mater. Process. Tech. (2011), doi:10.1016/j.jmatprotec.2011.06.011